Steady as She Goes: Reducing Flow-Induced Vibration in Hard Disk Drives

Industrial Representative: F. Hendriks (Hitachi GST)

Faculty: K. Black (Union College), R.J. Braun (Delaware), C. Breward (Oxford, UK), D. Duffy (NASA/GSFC, Retired), L. Mahadevan (Harvard), J. Ockendon (Oxford, UK), C. Please (Southhampton, UK), D. Schwendeman (RPI), B.S. Tilley (Olin College)

Students: D. Boy (Olin College), M. Franklin (Claremont), Z. Kurtz (Delaware)

Summary Presentation: R.J. Braun, 16 June 2006.

Report Preparation: R.J. Braun, D. Schwendeman, and B.S. Tilley

1   Introduction

Making smaller and less expensive disk drives is critical for success in many consumer electronic devices. One aspect that is under constant examination for improvement is steady flight of the disk heads. They fly only nanometers above the disks which are rotating at 7200 rpm or more. While the spinning of the disks and the viscous entrainment of the air within the drive allows the heads to fly, it also creates dynamic secondary flows that may buffet the head. This may necessitate the design of more sophisticated controllers to combat induced vibration or limit how narrow a track may be.

It seems reasonable that one can design the internal structure of the disk drive to mitigate the effects of these secondary flows. The flow in the drive had been investigated to some degree already using direct solution of the Navier-Stokes equations using proprietary software at Hitachi. While it seems to be a very good model giving good understanding of the flow in the drive, it is rather computationally expensive, requiring weeks to run. The purpose of this problem was to investigate simpler models for use in designing an appropriate flow. Perhaps the main idea is compute a good solution for a diverter that causes a decreased flow past the read heads and thus reduces buffeting of the heads; Figure 1 illustrates the basic idea.

A number of ideas were proposed that are discussed below. These ideas included: a lumped parameter model for the flow inside the drive; change the head/suspension design to prevent shedding of vortices; insert a fluttering blocker to prevent shedding vortices from the head/suspension assembly; computing the results of diverter shapes using compressible Euler equation models; apply shape optimization algorithms to the solvers to try to design an optimal diverter. All but the first tried to simplify the problem by studying only a local area near where flow would be diverted from within the spinning disks, just upstream of the heads; this is the darkened region in Figure 2. The first approach modeled the whole drive with a small ode system calibrated with some known quantities from the drive.

What results we have will be presented in the following sections, followed by Discussion and Summary sections.
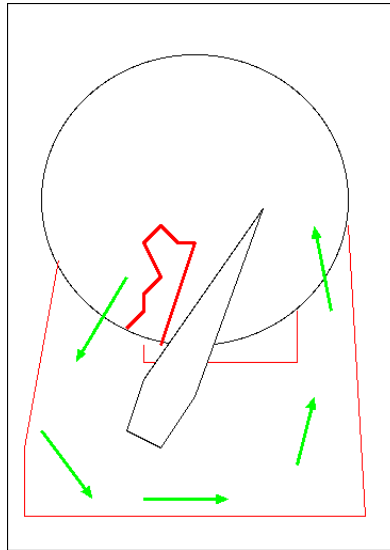
Figure 1: Sketch of disk drive and diverter purpose. The circle represents the counterclockwise spinning disks; there angular speed is ω. The long polygon to the right represents the arm that positions the heads; the irregular polygon represents the diverter, upstream of the heads, that diverts flow through the rest of the disk drive (arrows) in an effort to reduce buffeting of the heads.
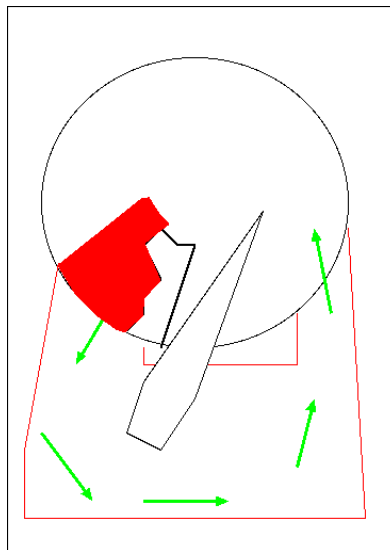
Figure 2: The computational models from the workshop for both the compressible inviscid and incompressible viscous models solve a problem in the darkened region indicated in the sketch.

2   A formulation

A sketch of the region of the disks away from the heads, but including the enclosure (shroud) around the disks; the space between the rotating disks can be viewed as a channel that drags
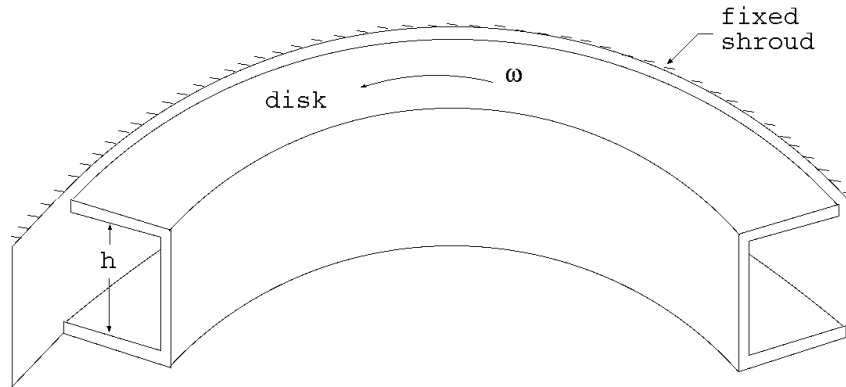
Figure 3: Sketch of part of disks away from the read/write heads and the including the shroud which does not rotate.

air around with this assembly as it rotates with angular speed ω. The separation between the platters, h, is 2mm. The Reynolds number is around 3000-7000 based on h. The azimuthal flow is basically rigid body rotation, but different in different horizontal sections. [I don't like the previous sentence; from that sentence it sounds like it's a shear flow, not rigid body rotation.] The flow between the disks is sketched in Figure 4. This sort of profile
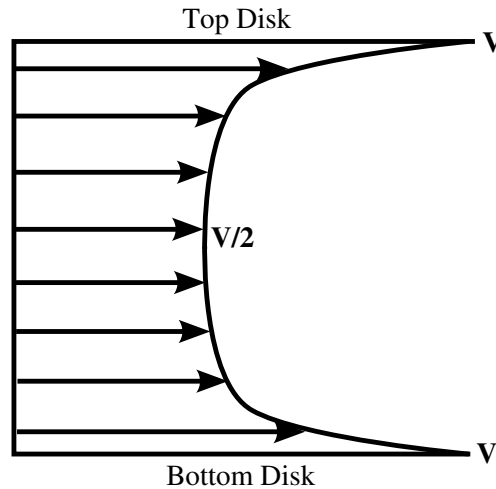
Figure 4: Velocity profile between the disks away from the read/write heads.

illustrates that diverting the flow away from the gap between the disks may not be as easy as it appears; the diverter certainly can't touch the disks, where the flow is fastest.

There are certainly categories of secondary flows, like Görtler vortices, where the flow leaves the disks and flows through the control and other mechanisms away from the disk.

Several formulations are attempted here. One is a circuit, or lumped parameter model for the drive. The remaining ideas involve inviscid flow. One involves changing the shape of the head/support structure to prevent vortex shedding. Computational models are also developed in the region indicated in Figure 2. One model will assume that the Reynolds number is large enough to treat the flow as a compressible inviscid flow for which the compressible Euler equations are solved. Finally, there are results from numerical solution of the incompressible Navier-Stokes equations.

3   Lumped parameter model

In this approach, the physical flow is reduced to a lumped parameter model in analogy with electric circuit models, and the complex space-time evolution of the actual system is approximated by discrete elements and ordinary differential equations. If the elements give a sufficiently close approximation to the system, then the model can be used to great effect. This approach is used successfully in vibration analysis [1], heat transfer and cooling of electronic equipment [2] and other applications.

In this problem, the analogy with electric circuits is given in Table 1. The following

Electric	Hydraulic
Voltage drop, $V = IR$	Pressure drop, $p = qr$
Voltage, $[V] = V$	Pressure, $[p] = Pa$
Current, $[I] = A$	Volume Flux, $[q] = \frac{m^3}{s}$
Resistance, $[R] = \Omega$	Flow "Drag", $[r] = \frac{kg}{m^4 s}$

Table 1: The analogy with electric circuits; the units of the analogous quantities are given.

equivalent circuit approximates the disk drive. There are three paths for flow, with the middle part of the circuit representing flow that is diverted away from the rotating disks, particularly the part of the disks where the heads fly.

The airflow through a spinning hard drive can be modeled effectively by an analogy between an electric circuit and the hydraulic behavior of the air flowing through the hard drive device. The quantities are outlined Table 1: The effective circuit is shown in Figure 5. From Kirchhoff's laws, we are able to use the effective circuit to come up with the following dimensional system of equations

$$q = q_m + q_b,$$

$$\Delta p_1 = q_b r_b,$$

$$\Delta p_1 = \alpha \psi - \left(k_p \psi + \frac{\alpha}{\beta} \right) q,$$

$$\Delta p_1 = -\alpha(2\pi - \psi) + \left(r_m + k_p(2\pi - \psi) + \frac{\alpha}{\beta} \right) q_m,$$
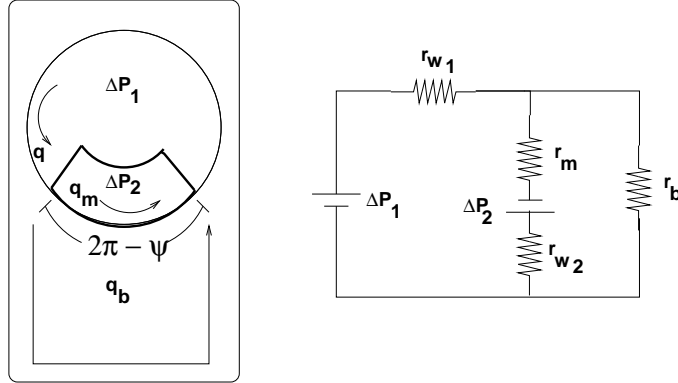
Figure 5: Effective circuit model. The hydraulic circuit of the air flow in the hard disk drive is shown at the right. The spinning disks produce an effective pressure drop that drives the flow q. Note that the angle ψ in the model describes the arc outside the "middle-channel".

by analyzing the flow of air q through the entire device, around the bottom loop, around the upper loop, and through the center, respectively. The physical resistance of the bypass is r_b, the pressure drop across r_{w2} is given by $k_p\psi q$ (where k_p is a proportionality constant so that $r_{w2} \propto \psi$), and the introduction of pressure to the system by the pump is given by $\alpha(\psi - q/\beta)$. The parameter β represents the "mass flux" through the device which is given by

$$\text{Mass Flux} = \int_{R_0}^{R_1} V \cdot H dr = H \int_{R_0}^{R_1} \omega r dr = \frac{1}{2}H\omega(R_1^2 - R_0^2),$$

where the radii R_0 and R_1 represent the inner and outer radii of the hard drive, respectively.

As shown in Figure 6 we rescale the variables as

$$q = \beta\bar{q},$$
$$\Delta P_1 = [p] = \alpha\bar{p},$$
$$r = k_p\bar{r},$$

where the overbar represents dimensionless variables. This leads to the following dimensionless system

$$\bar{q} = \bar{q_m} + \bar{q_b}, \tag{1}$$
$$\bar{p} = M\bar{q_b}\bar{r_b}, \tag{2}$$
$$\bar{p} = \psi - (1 + M\psi)\bar{q}, \tag{3}$$
$$\bar{p} = -(2\pi - \psi) + (M\bar{r_m} + M(2\pi - \psi) + 1)\bar{q_m}. \tag{4}$$

where the parameter $M \equiv k_p\beta/\alpha$.

From (4) we can find an equivalent expression for r_m

$$r_m = \frac{1}{M}\left\{\frac{\bar{p} + (2\pi - \psi)}{\bar{q}_m} - [M(2\pi - \psi) + 1]\right\} \tag{5}$$
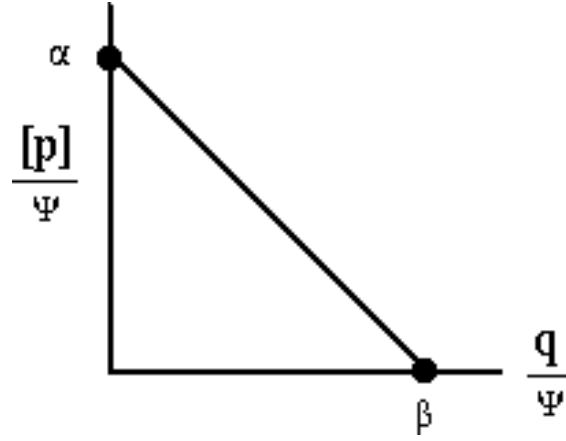
Figure 6: Air pumping characteristics of the spinning disks. Top: Pressure as a function of rotation rate. Bottom: Angle dependence.

The remaining equations (1)-(3) can be solved in terms of the flow in the middle section $\bar{q}_m$

$$\bar{q} = \frac{\psi + Mr_b\bar{q}_m}{1 + M\psi + Mr_b} \tag{6}$$

$$\bar{q}_b = \frac{\psi - (1 + M\psi)\bar{q}_m}{1 + M\psi + Mr_b} \tag{7}$$

$$\bar{p} = Mr_b\bar{q}_b . \tag{8}$$

With this and (5), we find that

$$r_m = \frac{r_b\psi}{\bar{q}_m\left[1 + M\psi + Mr_b\right]} - \frac{1}{M}\left\{\frac{2Mr_b\left[1 + M\pi\right] + (1 + M\psi)\left[1 + M(2\pi - \psi)\right]}{1 + M\psi + Mr_b}\right\} . \tag{9}$$

Since $r_m \geq 0$, this gives us an upper limit on the value of $\bar{q}_m$, which we call $\bar{q}^*$,

$$\bar{q}^* = \frac{Mr_b\psi}{2Mr_b\left[1 + M\pi\right] + (1 + M\psi)\left[1 + M(2\pi - \psi)\right]} . \tag{10}$$

The power P of the circuit is given by

$$P = (r_m + \psi)\,\bar{q}_m^2 + r_b\bar{q}_b^2 + (2\pi - \psi)\bar{q}^2 ,$$

which can with (6)-(9) be written in the form

$$P = A\bar{q}_m^2 + B\bar{q}_m + C , \tag{11}$$

where

$$A = \psi + \frac{\left[r_b(1 + M\psi)^2 + (2\pi - \psi)(Mr_b\psi)^2\right]}{(1 + M(\psi + r_b))^2} -$$
$$\frac{1}{M}\left\{\frac{2Mr_b\left[1 + M\pi\right] + (1 + M\psi)\left[1 + M(2\pi - \psi)\right]}{1 + M\psi + Mr_b}\right\} \tag{12}$$

$$B = \frac{r_b\psi}{\left[1 + M\psi + Mr_b\right]} + 2\frac{\left[Mr_b\psi(2\pi - \psi) - (1 + M\psi)r_b\right]}{(1 + M(\psi + r_b))^2} \tag{13}$$

$$C = \frac{\psi^2\left[r_b + 2\pi - \psi\right]}{(1 + M(\psi + r_b))^2} . \tag{14}$$

The optimization problem can then be phrased in the following way: Given a prescribed power level $P^* = A\bar{q}^{*2} + B\bar{q}^* + C$, where q^* is found in (10), find a $\bar{q}_m$ such that $P = P^*$ and $\bar{q}_m < q^*$. This problem requires, at least, that $A < 0$ and $P^* > C$, and its solution is given by

$$\bar{q}_m = \frac{B}{|A|} - \bar{q}^* > 0 .$$

To better describe this process, recall that in the case without an obstruction ($r_m = 0$) the air flows more easily in the disks than through the remainder of the casing, or $r_b \gg r_w$. This ansatz leads to the following asymptotic forms,

$$r_b = \frac{r}{M} , M \to 0 , \tag{15}$$

and $r_m = O(1/M)$. Using (15) in (11), we find

$$-r(2r + 3)\,\bar{q}_m^2 + \left[\psi(1 + r) - 2\right]\bar{q}_m + \psi^2 = 0 . \tag{16}$$

A typical graph of the power as a function of the middle air flow rate $\bar{q}_m$ is shown in Figure 7a. Notice that the reference power level is given with $\bar{q}_m = \bar{q}^*$, and that a smaller flow rate exists which gives the same power level. In Figure 7b, we show the equivalent graph but with the effective additional middle resistance Mr_m shown along the vertical axis.

Hence, this lumped parameter model suggests that there is a resistance that will both lower the flow around the reader arm with potentially a small power cost. The remaining sections of the report discuss how to determine the connection between the fluid mechanics and this resistance, and if there are other effects which mitigate the viability of this model.

4   Compressible Navier-Stokes Model

In this section, we focus on small part of the flow field where the fluid is diverted from flowing with the rotating disks and is sent through the remaining area of the drive. The idea is to explore the trade off between getting more flow diverted *vs.* higher torque required to spin the disks. This is a serious design issue that can be explored more rapidly than for a full direct computation. Here we frame the question as follows: What function for the diverter shape, $f(y)$, will divert the most momentum out through the bottom outlet?

(a)   (b)
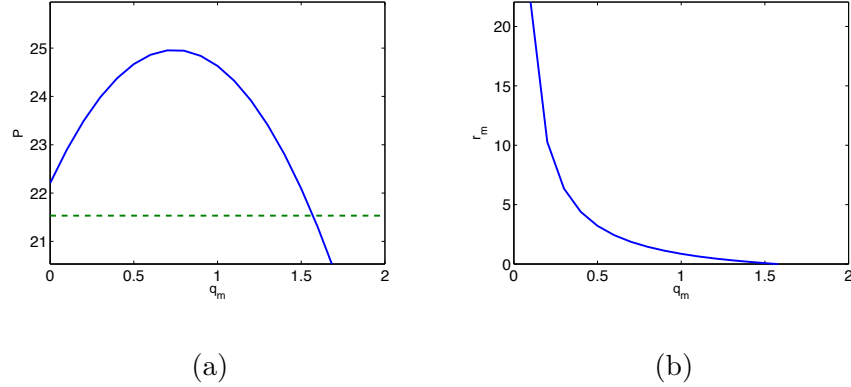
Figure 7: Plot of power levels (a) and effective middle-channel resistance r_m as a function of the flow rate through the middle section $\bar{q}_m$. The green dashed curve corresponds to the power P^*. Parameter values in this plot are $M \to \infty$, $r = 1$, and $\psi = 3\pi/2$.

For this optimization problem, consider the shaded region in Figure 2. We want to maximize the momentum through the bottom outlet:

$$\max_f \left\{ \int_{\text{outlet}} (\rho \vec{v}) \cdot \vec{n} \; ds \right\}. \tag{17}$$

At the same time we have constraints

$$\partial_t \rho + \nabla \cdot (\rho \vec{u}) = 0, \tag{18}$$

$$\partial_t (\rho \vec{v}) + \nabla \cdot (\rho \vec{v} \otimes \vec{u}) + \nabla P - \mu \nabla^2 \vec{u} - \frac{1}{3} \mu \nabla (\nabla \cdot \vec{u}) = 0, \tag{19}$$

$$\partial_t \left(p \rho^{1.4} \right) + \vec{u} \cdot \nabla \left(p \rho^{1.4} \right) = 0, \tag{20}$$

for isentropic flow, with appropriate boundary conditions.

The basic idea of the approach is to define a function based on the boundary, f,

$$J(f) = \int_{\text{outlet}} (\rho \vec{v}) \cdot \vec{n} \; ds \tag{21}$$

where f is from the set of permissible boundaries, V. If we are careful with our definitions then V is a Hilbert space with an associated inner product. Then we may use steepest descent method to optimize. In that case, we determine a search direction based on a gradient

$$J(f + w) = J(f) + <\text{Grad}_f J, w> + o(\|w\|), \tag{22}$$

for any $f, g \in V$. Choose

$$w = a \; \text{Grad}_f J, \tag{23}$$

where a is a free parameter, $0 < a \ll 1$. One can define a search direction based on a steepest descent scheme. This approach can be problematic because: (a) convergence can be slow; (b) choosing the free parameter may require multiple solves

An example of a local problem to which the shape optimization could be applied.

Results for this problem are shown in Figure 8. These computations show a developing layer by the diverter; further computations are needed in a geometry such as this.

A more promising approach may be to choose a search direction based on the "PDE Sensitivity Equation Method" (see [3])

5   Incompressible Navier-Stokes T-channel

The following results were found by Drs. Hendriks and Duffy using proprietary Navier-Stokes solvers. There is a series of results for a T-channel; the flow enters at the left; passing straight through corresponds to air following the disks. Flow turning down the other channel corresponds to being diverted away from the disks and heads and through the rest of the drive. The series of results that now follow have diverters at various angles, or no wall at all. The diverter in this sequence of results is a thin rectangular wall sticking out into the main channel at an angle of 30°, 60° or 90° with respect to the side wall of the channel.

The first result, shown in Figure 9 is for a T-channel without any diverter wall at all. The next results, shown in Figures 10 through 12, are for a T-channel with a diverter wall at 90°, 60° and 30° angles to the channel wall. Note that the diverter wall is constant length here. We see that the maximum diversion occurs for the 90° diverter. It seems likely that the optimum diversion came from the largest fraction of the straight channel being blocked by the diverter.

6   Inviscid Flow

Perhaps the biggest contribution from trying approaches like this was to use a local problem to try to design a diverter; this reduced the problem to a much smaller problem and more rapidly solved problem than that posed by a direct Navier-Stokes simulation of the whole disk drive.

6.1   Ideas from Complex Variables

In this subsection, we list some ideas that in principle employ complex variables.

One idea is to put a cross plate on the end of a splitter plate on the leading edge of the actuator arm, as illustrated in Figure 13. Complex variable methods could be used to design the plate and splitter to put a separating streamline as illustrated.

6.2   Compressible Flow

Compressible flow in a T-channel with various diverter geometries was considered. The flow is assumed to be inviscid and thus described by the Euler equations, which, for two-
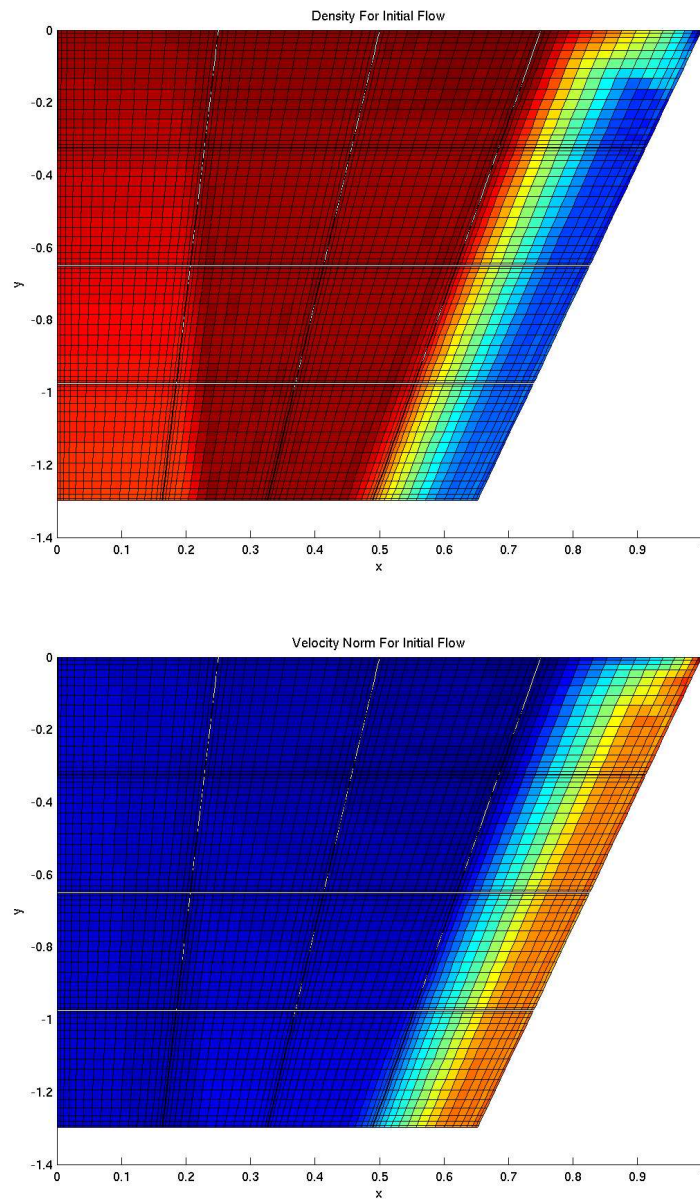
Figure 8: Density (top) and norm of the velocity (bottom) for a local computation near the diverter. The diverter in this computation is the inclined line at the right; the vertical line at the left edge is the shroud. The horizontal boundary at the top is an inlet from the spinning disk and the bottom boundary is the outlet into the rest of the drive away from the platters.
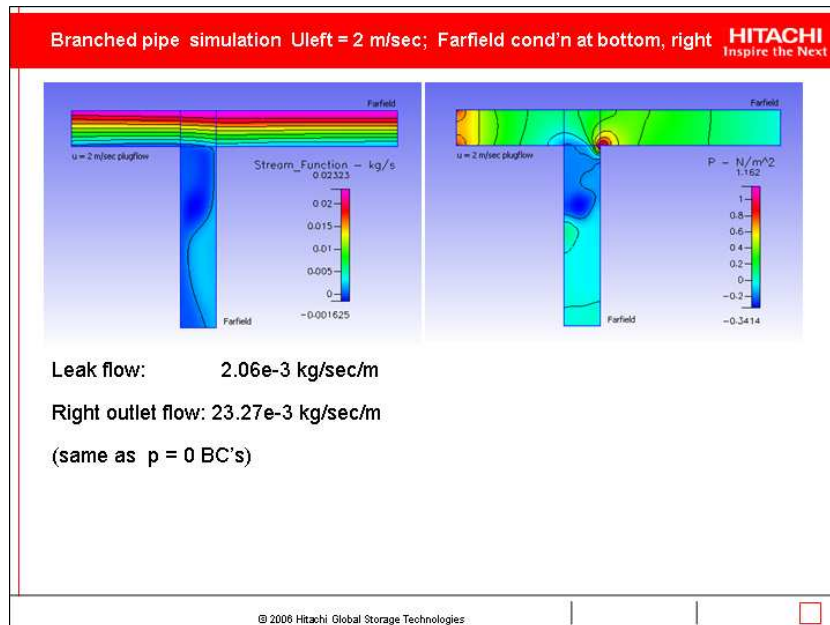
Figure 9: The flow in a model T-channel without any diverter. The mass flux diverted away from the main channel is small.
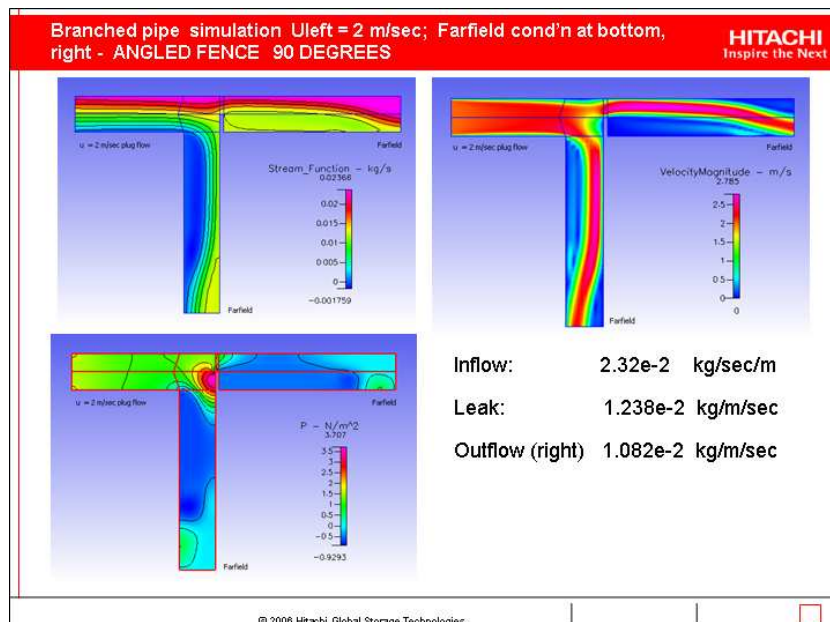
Figure 10: The flow in a model T-channel with a 90° diverter. The mass flux diverted away from the main channel is increased.
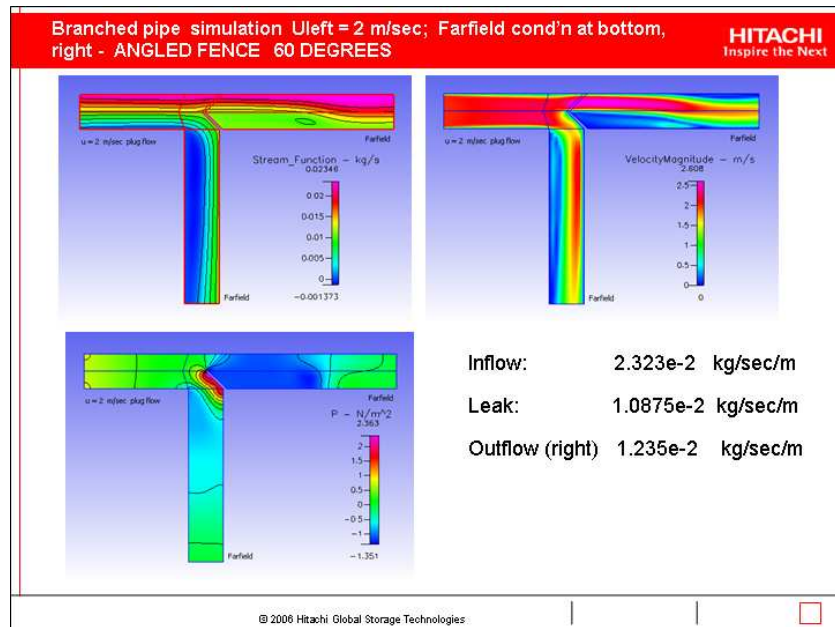
Figure 11: The flow in a model T-channel with a 90° diverter. The mass flux diverted away from the main channel is increased.
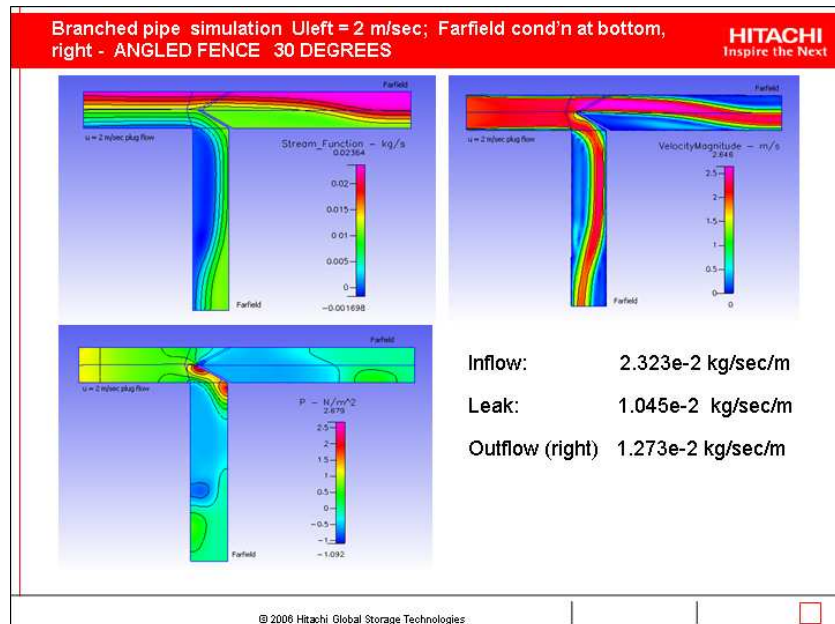
Figure 12: The flow in a model T-channel with a 90° diverter. The mass flux diverted away from the main channel is increased.

Cross plate

Separating Streamline

dead

Actuator arm

dead

U

Suggested length to
suppress vortex shedding
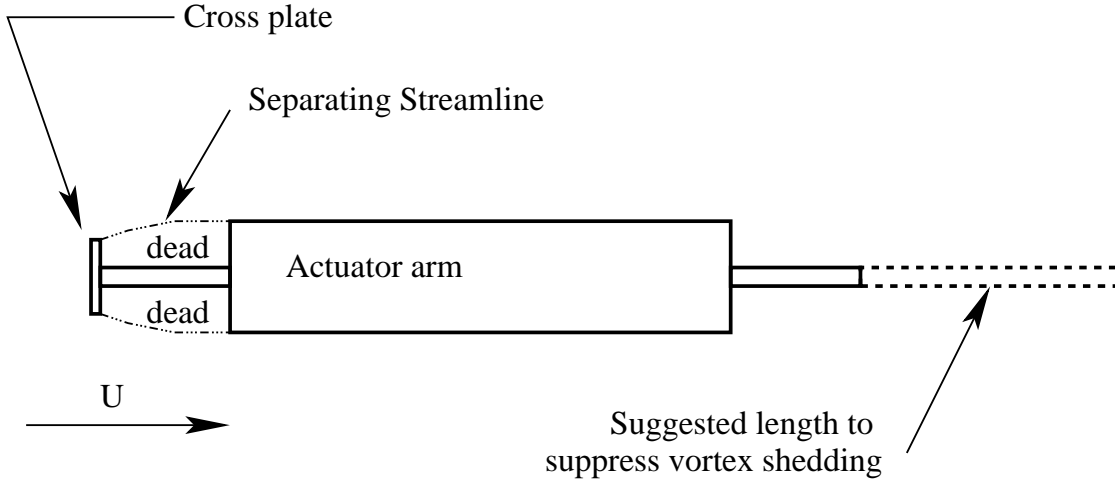
Figure 13: The splitter with a cross plate on the leading edge of the actuator arm
could be designed to have a separating streamline meet the corner of the actuator
arm. The splitter plate on the trailing edge (admittedly for viscous effects), could
eliminate vortex shedding.

dimensional flow, take the form

$$\mathbf{u}_t + \mathbf{f}_x(\mathbf{u}) + \mathbf{g}_y(\mathbf{u}) = 0,$$

where

$$\mathbf{u} = \begin{bmatrix} \rho \\ \rho u \\ \rho v \\ \rho E \end{bmatrix}, \qquad \mathbf{f}(\mathbf{u}) = \begin{bmatrix} \rho u \\ \rho u^2 + p \\ \rho uv \\ u(\rho E + p) \end{bmatrix}, \qquad \mathbf{g}(\mathbf{u}) = \begin{bmatrix} \rho v \\ \rho uv \\ \rho v^2 + p \\ v(\rho E + p) \end{bmatrix}.$$

The state of the flow at a position (x, y) and time t is given by $\mathbf{u}(x, y, t)$ which involves the
density ρ, the velocity (u, v) and the total energy E. The later has the form

$$E = \frac{p}{(\gamma - 1)\rho} + \frac{1}{2}\left(u^2 + v^2\right),$$

for an ideal gas with ratio of specific heats γ.

Numerical solutions of the Euler equations were obtained using the flow solver *CGCNS*
which is part of the *Overture* framework of codes [4]. The flow domain was discretized using
a composite overlapping grid which consists of a set of structured curvilinear grids that
overlap where they meet [5]. This discretization technique enables a smooth and accurate
representation of a wide range of complex flow geometries, including the ones considered
in this section. The governing equations are solved numerically using a time-dependent,
conservative, shock-capturing scheme. In this scheme, the numerical flux calculations are
performed using a second-order, slope-limited Godunov method with Roe-type approximate
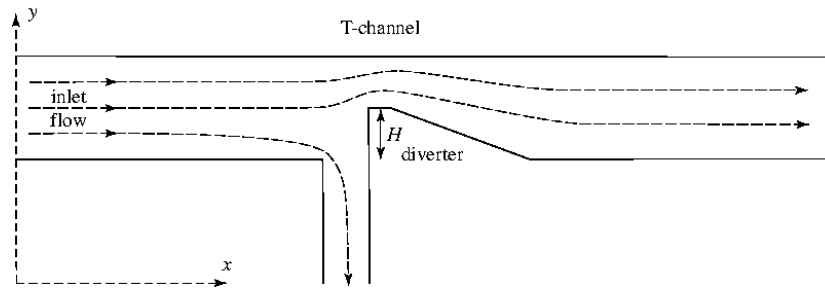
Figure 14: T-channel geometry with flow diverter.

Riemann solver [6]. The basic method of investigation of the flow was to choose a T-channel geometry with flow diverter and suitable initial conditions and boundary conditions (discussed below), and then integrate the governing equations numerically until the flow settled to steady state if one existed.

The T-channel geometry with flow diverter used in this study is shown in Figure 14. The gap height in the channel is normalized to 1 and the length of the channel is taken to be 8. A portion of the inlet flow on the left is diverted downward to a vertical channel of width 0.4 by a rigid diverter block of height H above the bottom wall of the T-channel. The flow in the region downstream of the diverter expands to accommodate a return to the original unit gap height of the channel. The flow enters the T-channel with velocity taken to be 0.2 in the x direction. The pressure of the inlet flow was normalized to 1 and the density was set to 1.4 so that the sound speed in the inlet flow is 1 (assuming $\gamma = 1.4$ for air). Thus the Mach number of the inlet flow is 0.2 which corresponds to a velocity of approximately 70 m/s.

Numerical calculations of the flow were performed for two values of H using a composite overlapping grid for each case. For example, the overlapping grid for the case $H = 0.5$ is shown in Figure 15. The overlapping grid consists of three component grids. There is a background Cartesian grid with grid spacings $\Delta x = \Delta y = 0.01$ for the bulk of the flow domain, and two boundary-fitted grids with similar grid spacings to handle the geometry of the flow diverter and vertical channel. It is noted that the sharp corners in the channel geometry are smoothed to eliminate any geometric singularities in the governing equations.

Let us first consider the long-time, steady state solution in the T-channel with flow diverter for $H = 0.5$. Figure 16 shows shaded contours of the density and the x and y components of velocity at $t = 120$. The plot of density shows that there is a relatively high compression in the flow as it accelerates around the upper tip of the diverter but that the value of density is close to initial value of 1.4 otherwise. The x component of velocity, u, is essentially zero in the downward diverter channel, and shows a transition from a value of 0.23, approximately, in the upper two thirds of the channel downstream of the diverter and a lower value of 0.13 in the lower third of the channel. The y component of velocity, v, is close to zero everywhere in the steady flow, except at the front of the diverter where there is a large positive value for v and the flow turns upward to round the tip of the diverter.
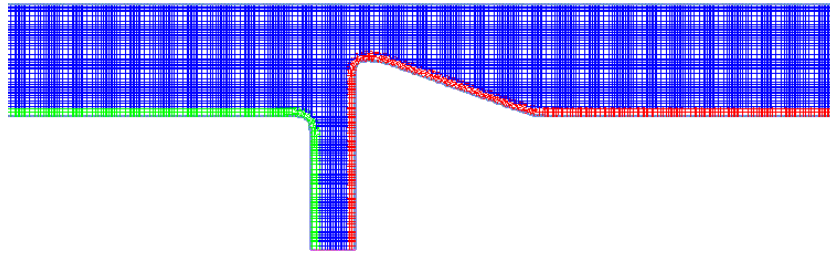
Figure 15: Composite overlapping grid for the T-channel geometry with flow diverter for $H = 0.5$.
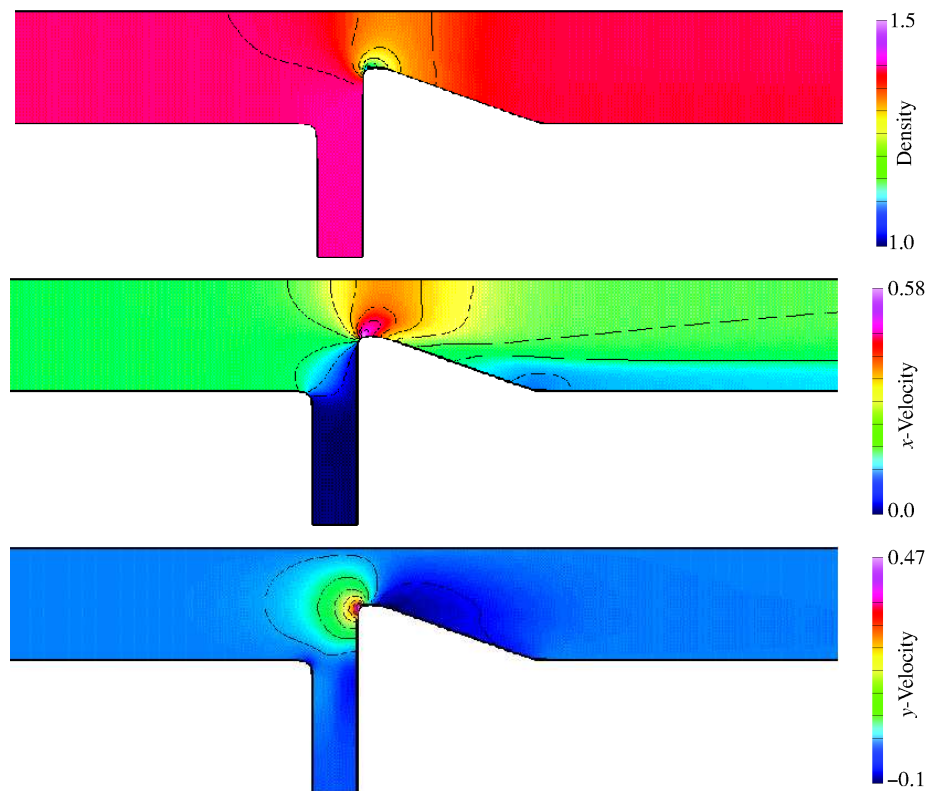
Figure 16: Steady state density and the x and y components of velocity for the T-channel geometry with flow diverter for $H = 0.5$.
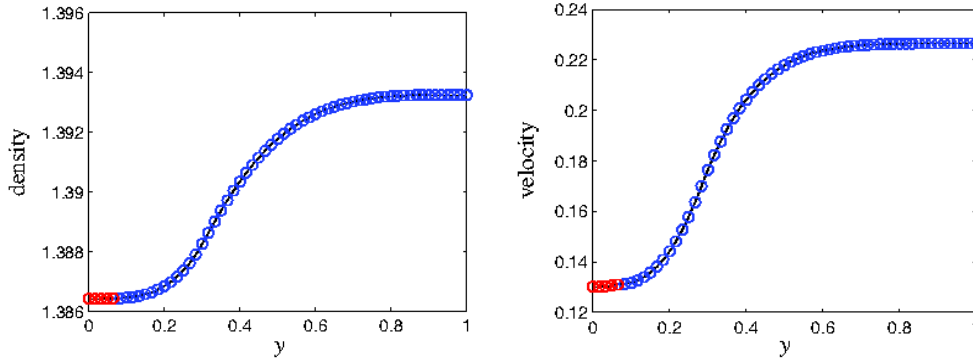
Figure 17: Density and the x-component of velocity at $x = 8$ for the T-channel geometry with flow diverter for $H = 0.5$.

The behavior of the density and normal component of velocity at the two outlets of the T-channel are shown in Figures 17 and 18. The solution at these locations may be used to determine the mass flow rate at each outlet. For example, the behavior of the flow at the outlet of the T-channel downstream of the diverter is shown in Figure 17. Here, we note that the density is nearly constant taking a value slightly less that its upstream value of 1.4 while the velocity shows a transition from $u = 0.13$ near the bottom of the channel at $y = 0$ to $u = 0.23$, approximately, near the top of the channel at $y = 1$. (The color of the marks in the figure correspond to the colors of the component grids in Figure 15 and thus indicate from which grid the solution is obtained.) The mass flow rate is computed using a numerical quadrature of the formula

$$Q_0 = \int_0^1 \rho(x, y) u(x, y) \, dy, \qquad x = 8,$$

and found to be $Q_1 = 0.2712$. In contrast, the behavior of the flow at the outlet of the downward diverter channel is shown in Figure 18, and these plots show very little variation in both the density and velocity, v. The mass flow rate here is given by

$$Q_1 = -\int_a^b \rho(x, y) v(x, y) \, dx, \qquad a = 3, \quad b = 3.4, \quad y = -1.2,$$

and found to be $Q_1 = 0.0088$. The sum of Q_0 and Q_1 equals the mass flow rate into the T-channel which is 0.28. Hence, for this channel geometry, only 3.1% of the mass from the inlet flow is diverted downward from the main flow stream.

A T-channel with a larger value of H for its diverter was considered to study the resulting flow behavior and to determine whether a larger fraction of the main flow stream could be diverter. For example, the behavior of the flow for the case $H = 0.75$ is shown in Figure 19. For this value it was found that the flow does not achieve a steady state due to vortices shed periodically from the upper tip of the diverter. The plots in the figure show the density at times $t = 192$, 198 and 204, and these are provided to give some indication of the unsteady
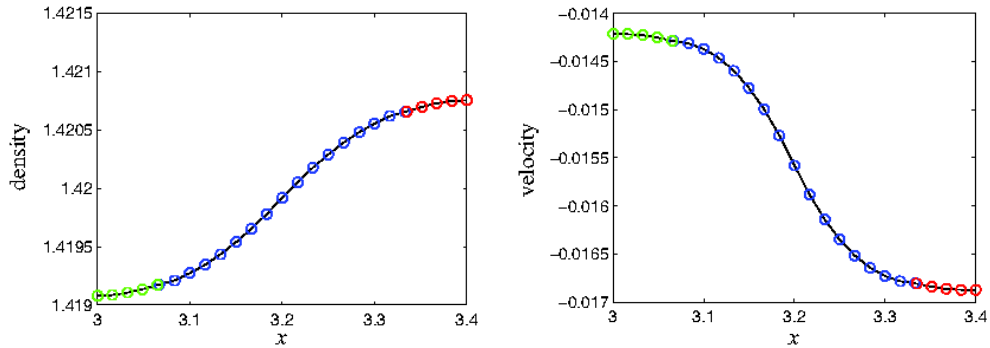
Figure 18: Density and the y-component of velocity at $y = -1.2$ for the T-channel geometry with flow diverter for $H = 0.5$.

behavior. This unsteadiness is considered to be undesirable for the downstream flow as it interacts with the read/write head and its support (not modeled in this simulation). Thus, we find a trade off between the desire to increase the mass flow rate in the diverted flow and unsteadiness of the main flow downstream of the diverter.

7   Fluttering Blocker

A suggestion was made by Dr. L. Mahadevan to consider an obstacle to be place ahead of the flying heads, between the disks, that fluttered and presumably disrupted the formation of von Karman vortices behind the disk heads. An illustration of the idea is shown in Figure 20. In favor of the idea is the existence of many flutter modes that could help destroy any vortices otherwise shed from the heads and high drag could help divert flow from the heads. On the other hand fabrication issues for device likely to be delicate and flexible could be daunting. Further, the frequencies at which the device would have to operate would be in the audible régime. The noise produced by the fluttering device eliminates this method to be used due to customer demands for quiet disk-drive operation.

8   Discussion

The methods to eliminate the flow between disks in a hard disk drive from impacting the reading of data has been significantly challenging. In this report, we note that the presence of an obstruction requires more power for the device. However, the lumped parameter model suggests that the power cost of the obstruction may not be that severe. A better quantitative study based on the effective values of the parameters to specific drives needs to be investigated in order to determine if this model is reliable.

The additional modeling rests on understanding the fluid flow in the region local to the diverter. In all cases the geometry of the diverter was simplified to a straight line at an angle from the unobstructed flow direction. Preliminary numerical results show that
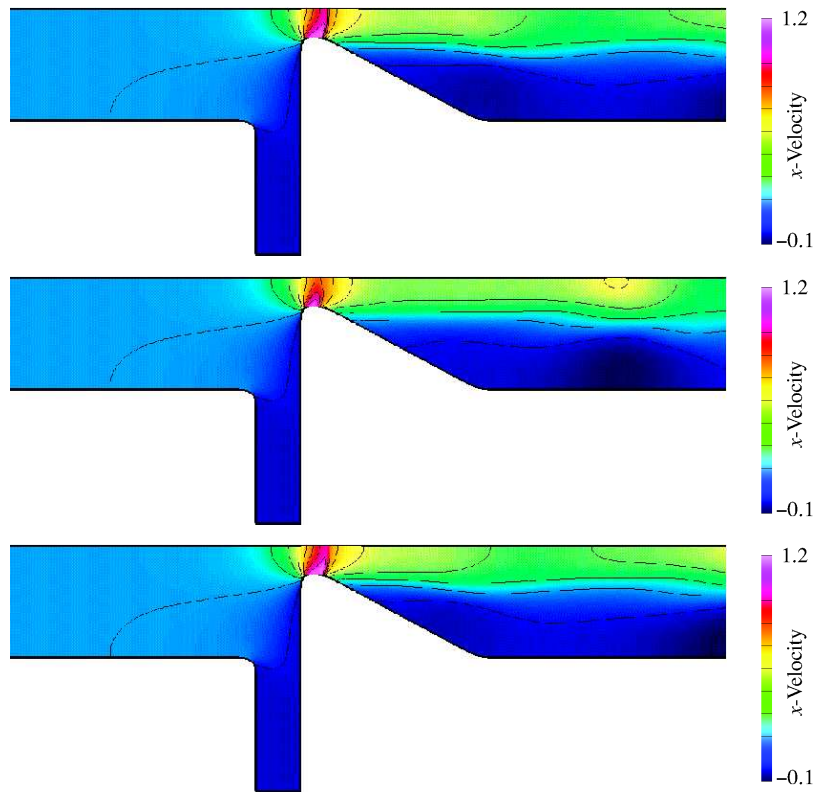
Figure 19: Time-dependent behavior of the x-component of velocity for the T-channel geometry with flow diverter for $H = 0.5$. Plot times from top to bottom are $t = 192$, 198 and 204.
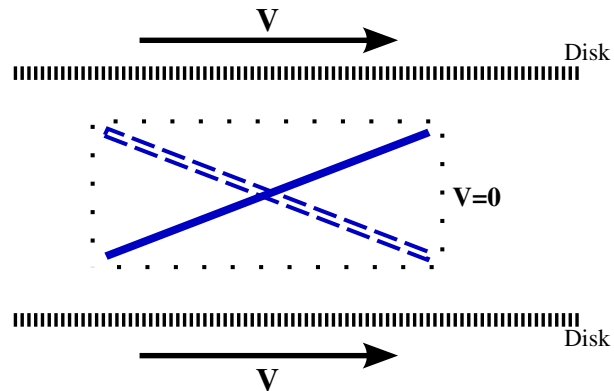
Figure 20: The mesh for the initial calculations; the mesh was generated with OGen.

Figure 21: The Ultrastar C10K147 hard disk (shown on the right) implements the flow diverter to help increase disk performance.

the flow can be diverted away from the reader arm appropriately. A steady Navier-Stokes simulation of a T-junction suggests that the best diverter angle is normal to the mean flow toward the diverter. However, a time-dependent investigation of Euler's equations suggests that minimizing the mass flow rate toward the reader arm induces unsteady behavior that propagates toward the reader arm. Such behavior could not have been predicted from a lumped parameter model.

In conclusion, a full study of the diverter shape to be used to minimize the buffeting felt by the reader arm from the unsteady flow is needed. Needless to say that this study is needed to help improve the design and performace of these hard disks. Between the workshop and the proceedings, Hitachi has come out with a server hard disk that implements this diverter idea (see Figure 21).

References

[1] L. Meirovich, Elements of vibraition analysis, McGraw-Hill, New York, 1980.

[2] A.D. Krauss, A. Bar-Cohen, Thermal analysis and control of electronic equipment, McGraw-Hill, New York: 1983.

[3] J. Borggaard and K. Burns, *J. Comp. Phys.* (1997).

[4] W. D. Henshaw, A primer for writing PDE codes with Overture, Tech. Rep. UCRL-MA-132231, LLNL (1998).

[5] G. Chesshire, W. Henshaw, Composite overlapping meshes for the solution of partial differential equations, J. Comp. Phys. 90 (1990) 1–64.

[6] W. D. Henshaw, D. W. Schwendeman, An adaptive numerical scheme for high-speed reactive flow on overlapping grids, J. Comput. Phys. 191 (2) (2003) 420–447.